

Supplementary Information

Virus transmission by aerosol transport during short conversations

Rohit Singhal, S. Ravichandran, Rama Govindarajan, Sourabh S. Diwan

Supplementary Text and Figures

1 Effect of inhalation on the flow pattern and aerosol transport

We have excluded inhalation from the speech cycles (figures 1c,d in the main text). To quantify the effect of inhalation on flow streamlines and the flux of aerosols carried by the streamlines, we perform the following exercise. We choose Case I, wherein Person 1, located at $(0, 0, 0)$, is a speaker, and Person 2 is a passive listener located at $(L_s, 0, 0)$ (figure 1a in the main text), and calculate the total aerosol flux reaching Person 2. We consider separately the effects of inhalation by the listener and by the speaker, finding both to be negligible.

1.1 Inhalation of the listener

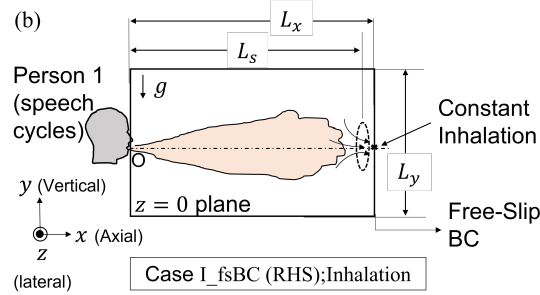


Figure S1: (**Inhalation of the listener**). Schematic representation of the computational domain for the set of cases denoted as “Case I_{fsBC(RHS);Inhalation}”. A constant suction of 0.1 l/s is applied at the orifice on the right-hand-side (RHS) face.

In principle, the breathing by the listener results in an approximate sinusoidal flow pattern, as given in Abkarian et al. (2020) and Giri et al. (2022). However, here we will consider the *average* effect of inhalation by the listener on the adjacent flow streamlines by prescribing a constant inhalation rate of 0.1 l/s. This is in the same spirit as done in the analysis of Yang et al. (2020) and by us for calculating inhaled virions in Eqs. (3) and (5) of the main text. To estimate the effect of the listener’s inhalation, we carry out simulations in which an orifice of diameter 2.45cm is located on the right-hand-side (RHS) boundary of the domain at $(L_x, 0, 0)$, at which the suction rate of 0.1 l/s is prescribed. A free-slip boundary condition is prescribed on the remaining face, as done for the simulations for Case II; see Fig. S1. Three different domain sizes are used for this exercise, with $L_s \in \{0.6\text{m}, 1.2\text{m}, 1.8\text{m}\}$ corresponding to L_x of $30d$, $55d$ and $80d$ respectively (including the offset of $\Delta \approx 0.15\text{m}$; $L_x = L_s + \Delta$, see the main text) and the lateral size fixed at $40d$. The grid resolutions used are 128^3 for $L_s = 0.6\text{m}$ and $256 \times 128 \times 128$ for the higher values of L_s . These grid sizes are found adequate for the present purposes; see section 2 below.

To understand the effect of using free-slip boundary condition on the flow near the RHS face, as against the open (or outflow) boundary condition used in Case I, we first prescribe zero inhalation velocity at the RHS orifice, i.e., effectively, a free-slip condition over the entire RHS face. We denote this set of simulations as “Case I_{fsBC(RHS);No Inhalation}” whereas Case I used in the main text is renamed as “Case I_{openBC(RHS)}” for the present discussion. Fig. S2 compares the aerosol exposure from the two cases over 140s, i.e., $F_I(L_s, y_s = 0, t_c = 140\text{s})$ as defined in Eqs. (1) and (2) in the main text. We find that the values of F_I for “Case I_{fsBC(RHS);No Inhalation}” are almost identical with those for “Case I_{openBC(RHS)}” for $L_s = 0.6\text{m}$ and 1.8m , and show a small deviation (less than 10%) for $L_s = 1.2\text{m}$ (Fig. S2). This provides support for the use of free-slip boundary condition on the RHS face for this exercise as well as for Case II simulations in the main text. The results for the constant inhalation of 0.1 l/s specified on the RHS orifice are also shown in Fig. S2 and are denoted as “Case I_{fsBC(RHS); Inhalation}”. As can

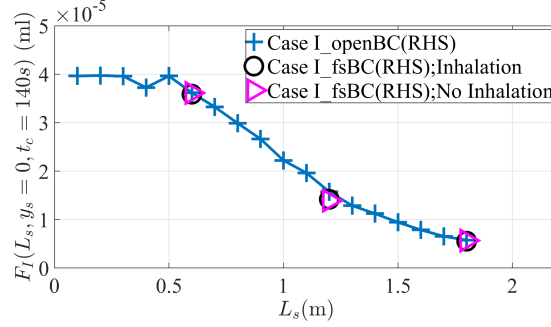


Figure S2: **(Inhalation of the listener).** The total scalar exposure to a silent listener with and without inclusion of inhalation. Note that “Case I_openBC(RHS)” is the same as Case I described in the main text and uses open boundary condition on the RHS face. The other two cases use a free-slip boundary condition, except when a suction rate of 0.1 l/s is prescribed at the RHS orifice.

be seen, the presence of inhalation does not make any perceptible difference in the values of F_I as compared with “Case I_fsBC(RHS);No Inhalation”, for all the three values of L_s . This is because the inhalation alters the flow-field over only a small portion near the orifice (or “mouth”, as seen in Fig. S3) and therefore has a minimal effect on the integrated aerosol flux across the face, F_I , seen in Fig. S2. This further justifies our use of the entire face as a potential receptacle for infection. The small differences in the streamline patterns away from the orifice in Figs. S3(a) and (b) are due to statistical variations, present inherently in instantaneous quantities. We expect that the effect of prescribing any typical inhalation-exhalation cycle for the listener (e.g. the one in Giri et al., 2022) will be of the same order as that of constant inhalation studied here and that the values of F_I (which are integrated over an area of diameter 17.2cm) should be largely insensitive to these variations.

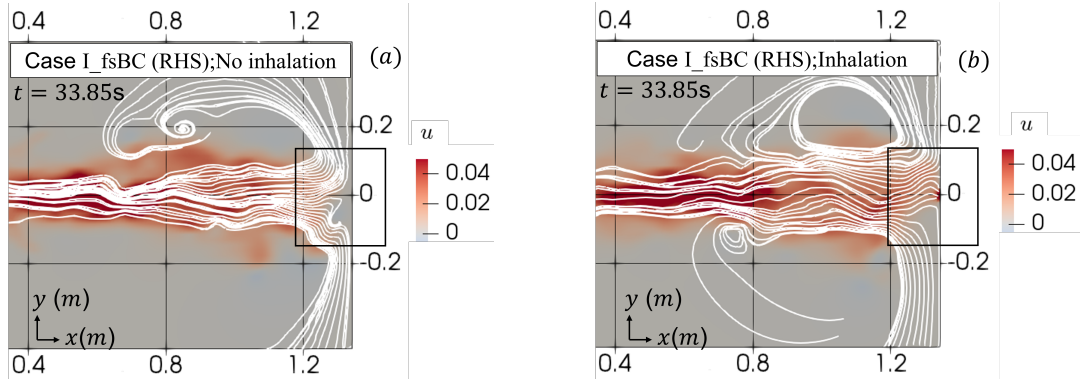


Figure S3: **(Inhalation of the listener)** A slice through $z = 0$ showing instantaneous axial velocity contours and streamlines in the $x - y$ plane for (a) “Case I_fsBC(RHS); No Inhalation” and (b) “Case I_fsBC(RHS); Inhalation”. The computational domain is $55d \times 40d \times 40d$ (corresponding to $L_s = 1.2m$). The square boxes highlight the difference in the flow field near the orifice on the RHS face with and without suction.

1.2 Inhalation of the speaker

For this study, we include inhalation in the speech cycle of the speaker located on the left-hand-side (LHS) face of the domain (Person 1). The resulting speech pattern is shown in Fig. S4 and is identical with that used in Abkarian et al. (2020) for the speech phrase “Peter Piper picked a peck”. The intermittent inhalation results in relatively strong vortices near the orifice which tends to lead to a solution blow-up, since the orifice exit corresponding to the speaker mouth is aligned with the LHS face in the present set-up. This issue is likely to be less severe for the set-up used in Abkarian et al. (2020), who have used a semi-hemispherical projection to mimic the human head. The problem occurs primarily because of the use of free-slip boundary condition on the LHS boundary in our simulations which we resolve by introducing a viscous padding over a certain region near the LHS face. This is consistent with Giri et al. (2022), who have a similar set-up as ours but have used no-slip boundary conditions on the left and right faces in their simulations, except for the orifice.

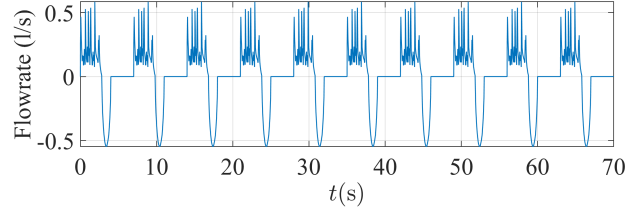


Figure S4: **(Inhalation of the speaker)** The speech cycles used for the speaker on the left-hand-side face of the domain (Person 1) for evaluating the effect of presence of inhalation on the flow field. The duration of inhalation is 1.2s (Abkarian et al. 2020).

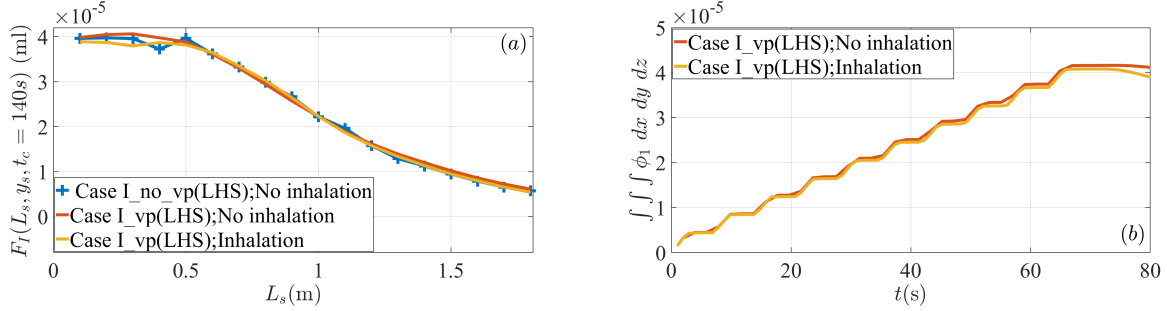


Figure S5: **(Inhalation of the speaker)** (a) Total scalar exposure at different downstream locations with and without presence of inhalation in the speech cycles for Person 1. The effect of using viscous padding (denoted as “vp”) on the LHS face is also assessed. Note that “Case I_no_vp(LHS); No Inhalation” is the same as “Case I” used in the main text. (b) Total amount of aerosol present in the domain as a function of time with and without inhalation.

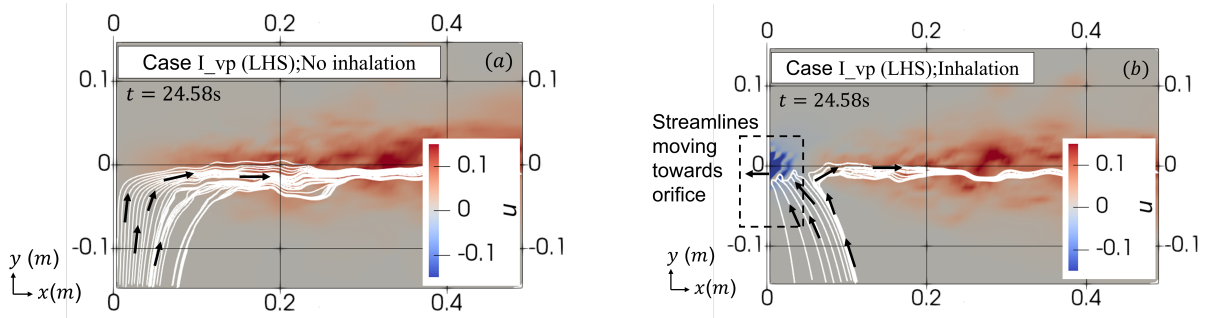


Figure S6: **(Inhalation of the speaker)** A slice through $z = 0$ showing instantaneous axial velocity contours and streamlines in the $x - y$ plane for (a) the case with no inhalation in the speech cycles, (b) the case with inhalation included in the speech cycles (Fig. S4). The rectangle in (b) shows presence of negative axial velocities due the inhalation and the deflection of streamlines towards the orifice.

We first evaluate the effect of viscous padding by comparing the total aerosol flux with that in Case I which uses free-slip condition on the LHS face (and does not involve inhalation; Fig. 1 in the main text). The former case is denoted as “Case I_vp(LHS);No Inhalation” and the latter as “Case I_no_vp(LHS);No Inhalation”. The case involving inhalation in the speech cycle (as in Fig. S4) is denoted as “Case I_vp(LHS);Inhalation”. The domain size used for the simulations is $80d \times 40d \times 40d$ and the grid resolution is $256 \times 128 \times 128$. For this set of simulations, the boundary on the RHS face is prescribed as an open boundary. Fig. S5(a) shows that the presence of viscous padding near the LHS face does not alter the streamwise variation of the total aerosol flux, F_I , except for a small deviation around $L_s \approx 0.4m$. Furthermore, even the inclusion of inhalation affects the aerosol flux values only by a small amount for $L_s < 0.4m$, and beyond this distance the F_I profile is identical with that for the “No Inhalation” case (Fig. S5(a)). This is also evident from the total amount of aerosol present within the domain plotted in Fig. S5(b) as a function of time. The curves for the “Inhalation” and “No Inhalation” cases (with viscous padding on the LHS face) show a close agreement all the way until the end of speech duration (70s). To understand how inhalation in the speech pattern affects the flow field in the vicinity of the orifice, we plot instantaneous streamlines (in the lower half of the $x - y$ plane) overlaid on

the streamwise velocity contours in Fig. S6. As can be seen, inhalation affects the flow field only in the immediate vicinity of the orifice and the reverse flow induced due to suction does not extend beyond $x \approx 0.1\text{m}$ (Fig. S6(b)). Thus the presence of inhalation is not expected to contribute to the aerosol transport beyond this distance in any significant way, as is evident from Fig. S5. The reason for this is that fluid dynamics operating in blowing (exhalation) is different from that in suction (inhalation) in inertial flows; whereas the former results in a directed jet advancing downstream with ease, the latter creates a sink, drawing in air from a hemispherical region around the orifice (Abkarian et al. 2020). So, the momentum flux across a given cross-sectional area directly downstream of the mouth is much smaller during inhalation than during speech.

To summarize, we have shown that inhalation introduced either on the side of the listener or on the side of the speaker has insignificant effect on the directed aerosol transport, which is the main variable we use for calculating the risk of virion ingestion. This provides a justification for the exclusion of inhalation in the speech cycle for the simulations presented in the main text.

2 Details on the grid-resolution exercise

Fig. S7 presents the streamwise variation of the cycle-averaged centreline velocity (for Case I) for three different grid sizes, namely, 1024^3 , 512^3 and 256^3 , and for a cubical domain of $70d^3$. This is the first part of the grid-resolution exercise described in section 2.2 in the main text. Figs. S8-S12 present the outcome of the second part of this exercise, wherein we use two grid resolutions of $256 \times 128 \times 128$ and $512 \times 256 \times 256$, each for domain sizes of $80d \times 40d \times 40d$ (for case I) and $55d \times 40d \times 40d$ (for Case II). More detailed comments on the comparison specific to a given plot are made in the figure captions.

2.1 Calculation of dissipation of turbulence energy and Kolmogorov length scales

The dissipation rate of turbulence kinetic energy (ϵ) at a given time instant is calculated as (Pope, 2000)

$$\epsilon(x, y, z, t) = \nu \left[2 \left(\frac{\partial u}{\partial x} \right)^2 + 2 \left(\frac{\partial v}{\partial y} \right)^2 + 2 \left(\frac{\partial w}{\partial z} \right)^2 + \left(\frac{\partial v}{\partial x} + \frac{\partial u}{\partial y} \right)^2 + \left(\frac{\partial w}{\partial y} + \frac{\partial v}{\partial z} \right)^2 + \left(\frac{\partial u}{\partial z} + \frac{\partial w}{\partial x} \right)^2 \right]. \quad (\text{S1})$$

The Kolmogorov length scale is typically calculated based on a suitably-averaged dissipation rate. Since we wish to obtain the variation in time of the Kolmogorov scale, we prefer not to carry out averaging over speech cycles in this exercise. We instead carry out an azimuthal averaging in $\theta = \tan^{-1}(y/z)$, at a given radius, $r = \sqrt{(y^2 + z^2)}$, and denote the averaged dissipation rate as $\bar{\epsilon}(x, r, t)$. The Kolmogorov length scale at given x is then calculated using a maximum in $\bar{\epsilon}$ over all r , $\bar{\epsilon}_{max}(x, t)$, as

$$\bar{\eta}_K(x, t) = \left(\frac{\nu^3}{\bar{\epsilon}_{max}(x, t)} \right)^{1/4}. \quad (\text{S2})$$

The resulting variation of $\bar{\eta}_K$ in x at different time instants for the speech flow in Case I is plotted in Figs. S9(a-c) for the grid sizes of $256 \times 128 \times 128$ and $512 \times 256 \times 256$. Also included in Fig. S9(c) is the line $\bar{\eta}_K = 0.0032x$ obtained from the measurements of Panchapakesan and Lumley (1993). The derivation of this relation is presented below.

Panchapakesan and Lumley (1993) obtained estimates of the dissipation rate in a round turbulent jet from the energy budget equation as a balance; the other terms in the equation were directly measured using hotwire anemometry. They found the time-averaged dissipation to attain a peak of $\bar{\epsilon} = 0.017U_c^3/\delta_{1/2}$ close to the axis of the jet, where U_c is the jet centreline velocity and $\delta_{1/2}$ is the “half-width” of the jet (i.e., the radial distance at which the local axial velocity is $U_c/2$). Note that we use the same symbol, $\bar{\epsilon}$, to represent time- and azimuthal averaged dissipation, for convenience. We use the following self-similar relation for U_c (we neglect the distance between our origin and the virtual effective origin of the jet).

$$U_c = \frac{BU_o}{(x/d)}, \quad (\text{S3})$$

where U_o is the orifice exit velocity. Panchapakesan and Lumley (1993) obtained $B = 6.06$ and $\delta_{1/2} = 0.096x$. Using these values and equation (S3), we get

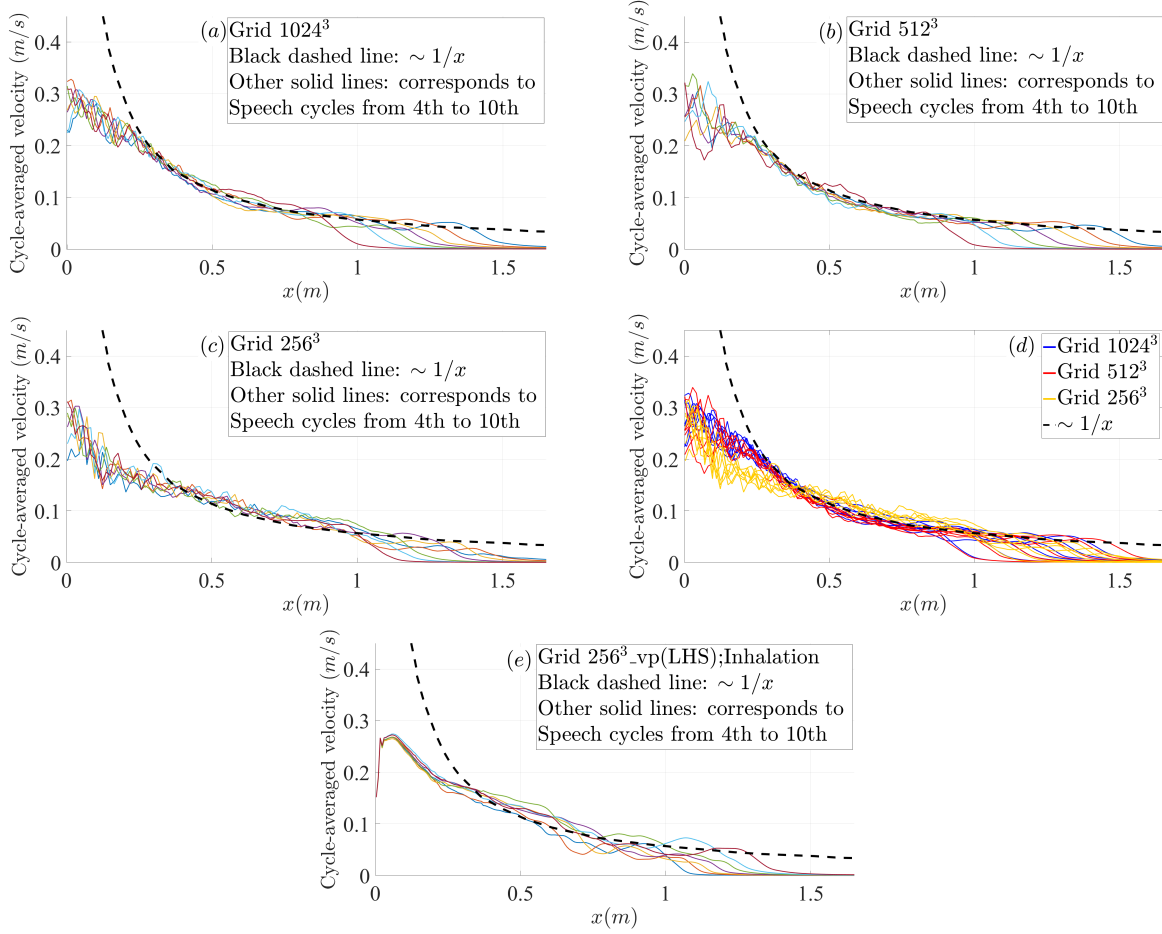


Figure S7: (Grid-resolution and validation exercise) Cycle-averaged centreline velocity versus axial distance (in m) for the grids: (a) 1024^3 (b) 512^3 and (c) 256^3 , for Case I. The simulation domain used for this exercise is $70d^3$ and each speech cycle consists of 2.8s of speaking the phrase “Peter Piper picked a peck” with 1.2s of silence. This is similar to what is used in Abkarian et al. (2020), except that the inhalation phase is replaced with zero velocity. The black dashed line represents the $1/x$ curve which is typical of the steady self-similar round jet. Other lines show the averaged centreline velocity corresponding to a given cycle number (4^{th} to 10^{th}). (d) Grid-convergence of the cycle-averaged velocity. As can be seen the cycle-averaged centreline velocity follows the $1/x$ variation for $x \gtrsim 0.4m$ until about $1 - 1.4m$ (depending upon the cycle number used for averaging) for all the grid resolutions. Moreover, the difference among the three resolutions is small in this region. The departures from the $1/x$ curve seen for small and large x are consistent with the observations in Abkarian et al. (2020; their Fig. 5D). The undulations observed in the data close to the orifice ($x = 0$) are due to the fact that the data are saved at coarser time intervals and therefore there are statistical fluctuations in that region. These wiggles are not a result of insufficient grid spacing as these are seen even for the largest grid resolution. (e) Cycle-averaged centreline velocity versus axial distance with inhalation included, i.e., for the speech cycle consisting of 2.8s of speech and 1.2s of inhalation (akin to that in Fig. S4 except for the quiescent part). This case is denoted as “Grid 256^3 _vp(LHS);Inhalation” as viscous padding has been used on the left face as discussed above in section 1.2. As expected, inhalation causes a reduced centreline velocity near the orifice as compared to that in (c) which does not include inhalation. Note that the effect of presence of inhalation is felt only over a distance of $\approx 0.1m$ from the orifice, consistent with the analysis in section 1.2 (see Fig. S6). The overall variation of the cycle-averaged velocity for the present case is consistent with that reported in Abkarian et al. (2020). There are small quantitative differences near the orifice which are due to the different boundary conditions prescribed on the left face in the two studies. While we use free-slip boundary condition on a planar surface with viscous padding, Abkarian et al. (2020) specify zero-velocity Dirichlet condition on a spherical surface mimicking human head.

$$\bar{\epsilon} = 39.4U_o^3 d^3 / x^4. \quad (S4)$$

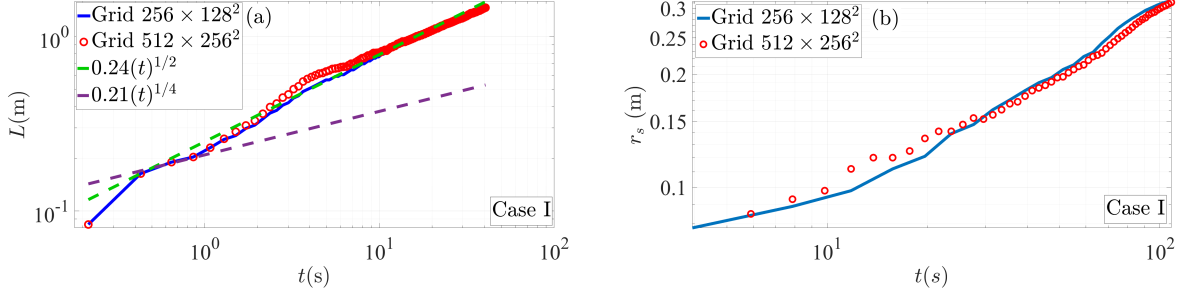


Figure S8: (Grid-resolution and validation exercise) (a) Evolution of the axial extent of the flow, the “length”- (L), as a function of time (t) for Case I. The flow length is determined as the distance from the orifice which covers 90% of the total aerosol concentration (Abkarian et al. 2020). The lines $0.24(t)^{1/2}$ and $0.21(t)^{1/4}$ represent the behavior of L for a starting jet and puff respectively, similar to the reported results in Abkarian et al. (2020). The evolution of the speech flow from a puff behavior to jet behavior is clearly seen. This provides a further validation to the present simulation results. (b) Variation of the lateral (radial) width, r_s , of the speech flow with time, as defined in Section 4 in the main text; see equation (9). Results from the two grid resolutions are included in (a) and (b); the grid refinement does not change the quantitative variation of these quantities much, except for a small deviation around $t = 4$ s in (a) and $t = 10$ s in (b).

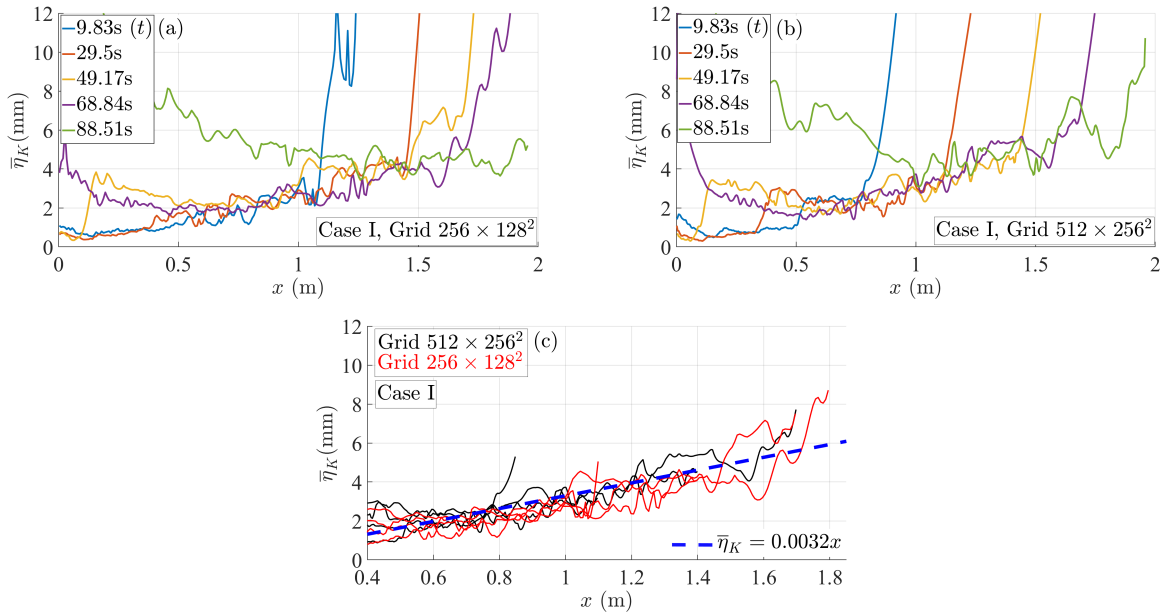


Figure S9: (Grid-resolution and validation exercise) Streamwise variation of the Kolmogorov length scale $\bar{\eta}_K$ (averaged in the azimuthal direction and based on the maximum dissipation rate at a given x) at different time instants for Case I for two grid resolutions: (a) $256 \times 128 \times 128$, and (b) $512 \times 256 \times 256$. $\bar{\eta}_K$ is calculated from equation (S2). The values of $\bar{\eta}_K$ are seen to be largely independent of the grid size used, which implies that the grid size of $256 \times 128 \times 128$ used for the results in main text is adequate for capturing the dissipation of turbulence kinetic energy with a sufficient level of accuracy. (c) Comparison of the computed $\bar{\eta}_K$ (at selected time instants) for the quasi-steady regime of the speech jet with the variation, $\bar{\eta}_K = 0.0032x$ (equation S6) obtained from measured dissipation values for a steady round jet by Panchapakesan and Lumley (1993); for more details, see section 2. There is an excellent match between the measured and computed variations of $\bar{\eta}_K$ for both the grid resolutions over the quasi-steady regime ($0.45m < x < 1.4m$), except for statistical fluctuations. Note that the cycle-averaged values of $\bar{\eta}_K$ can be expected show a smoother variation with x than seen in (c).

Equation (S4) in conjunction with equation (S2) gives

$$\bar{\eta}_K = 0.4x(Re_o)^{-3/4}, \quad (S5)$$

where $Re_o = (U_o d)/\nu$ is the Reynolds number based on the orifice conditions. In the present work, the orifice velocity varies in time (figure 1(c) and (d) in the main text) so we use the average velocity at the orifice ($= 0.379\text{m/s}$; averaged over the exhalation part of the speech cycle) for U_o and the effective orifice diameter ($= 2.45\text{cm}$) for d , to obtain $Re_o = 619$. Using this value of Re_o in equation (S5) we get, for present conditions,

$$\bar{\eta}_K = 0.0032x. \quad (S6)$$

2.2 Comparison of the present grid spacing with that reported in the literature

Here we compare grid resolution in the present DNS with that reported in the literature. Towards this, we include the DNS studies on cough flows by Chong et al. (2021) and Rosti et al. (2021), and the DNS of speech flows (conversation) by Giri et al. (2022). We include both the grid resolutions used in the present exercise: $256 \times 128 \times 128$ (corresponding to the results in the main text - “normal grid”) and $512 \times 256 \times 256$ (finer grid). To adjust for the differences in Reynolds numbers (and also in orifice diameters) used in these studies, we refer all the grid spacings (Δ) to the Reynolds number of the present study, using the commonly used relation (obtained from Kolmogorov arguments): $\Delta/d \propto (Re)^{-3/4}$. This provides a common basis for comparing the present grid spacing with those reported by others. Towards this, we use the following equation

$$\frac{\Delta_{derived}}{\Delta_{others}} = \frac{d_{present}}{d_{others}} \left[\frac{Re_{present}}{Re_{others}} \right]^{-3/4}, \quad (S7)$$

where, $\Delta_{derived}$ is the grid spacing corresponding to our Reynolds number, *derived* from the grid spacings reported by others. In other words, $\Delta_{derived}$ represents an equivalent grid resolution in a given DNS study, if it used the same Reynolds number as ours. The outcome of this exercise is presented in Table S1. We find that our grid resolution (“normal grid”) is better than those of Chong et al. (2021) and Rosti et al. (2021), given the much smaller Reynolds number used here. On the other hand, it is coarser than that used by Giri et al. (2022). We note that our grid resolution is able to accurately capture the turbulence dissipation rate (Fig. S9) and estimate the viral load correctly.

Table S1. Comparison of the grid spacing in the present study with that of other DNS studies reported in the literature. By “Normal Grid” we mean the grid resolution that has been used for the results in the main text. U_m is the maximum orifice velocity and U_o is the mean orifice velocity (averaged over the cough duration or the exhalation part of the speech cycle). Note that Re_m used here is the same as Re used in the main text.

Studies		Chong et al.(2021)	Rosti et al.(2021)	Giri et al. (2022)	Present Study Normal Grid: $256 \times 128 \times 128$	Present Study Finer Grid: $512 \times 256 \times 256$
$Re_m = U_m d / \nu$		-	17290	1800-2000	1906	1906
$Re_o = U_o d / \nu$		16492	-	700	619	619
Grid size	$\Delta_x(\text{mm})$	0.703	1.75*	2.0	7.66 ($L_x = 80d$) 5.26 ($L_x = 55d$) 5.74 ($L_x = 30d$)	3.83($L_x = 80d$) 2.63($L_x = 55d$)
	$\Delta_{y,z}(\text{mm})$				7.66	3.83
$\Delta_{derived}$ (mm)	Based on Chong et al.(2021)	-	-	-	8.96	8.96
	Based on Rosti et al.(2021)	-	-	-	9.96	9.96
	Based on Giri et al.(2022)	-	-	-	2.19	2.19

* Finest grid used in grid convergence study by Rosti et al. (2021).

2.3 Comments on the deviation of results between two grid resolutions

Since the two grid resolutions used in the present exercise result in nearly the same values for energy dissipation, we would expect that the behavior of other quantities such as the length and width of the flow, and the aerosol flux should be practically unaltered between the two resolutions. Figs. S8-S12 show that although these quantities (and in particular the total aerosol exposure and viral dose) are most often in close agreement with each other, there are regions over which the difference between them is $\sim 10\%$. In this connection, we refer to a similar exercise performed by Abkarian et al. (2020; see their Supplementary Information) who carried out additional simulations with a finer grid and with slightly different initial conditions. They found that the jet spread angles varied in the range $0.189 - 0.233$ rad for these simulations, and the length of the speech flow showed deviations similar to what we observe here; compare Fig. S8(a) below with Fig. S2 from Abkarian et al. (2020). Abkarian et al. estimated these deviations to be of the order 10% and attributed them to the statistical variations between individual realizations of the inherently transient speech flows. It is noteworthy therefore that the minor deviations between simulations at different grid resolutions include the effects of statistical flow variations which are of the same order, and further grid resolution may not serve any purpose. To separate out the two factors we need to perform ensemble averaging over several realizations for a given speech flow (Abkarian et al. 2020), which is beyond the interest area of the present work.

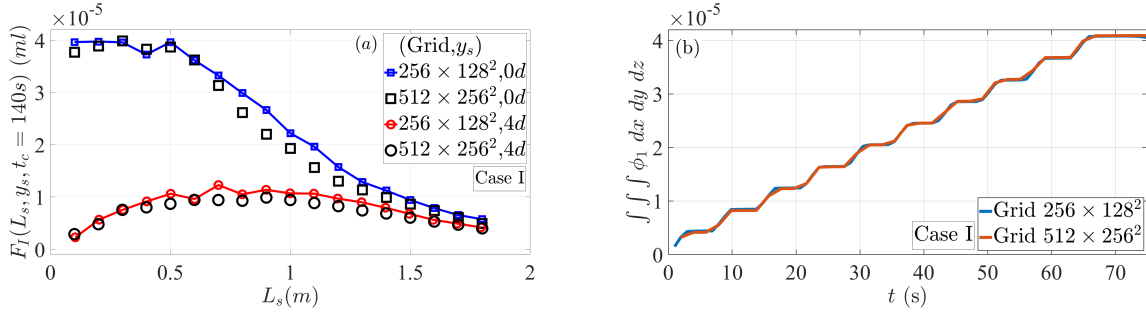


Figure S10: **(Grid resolution exercise)** (a) Total scalar exposure F_I over 140s to a silent listener located at different streamwise distances (L_s) from the speaker for Case I. F_I is defined in equations (1) and (2) in the main text. Results from two grid resolutions are included, and for each grid size two different vertical separations (y_s) are used. The maximum deviation between F_I values for the two grid resolutions is of the order 10% for $L_s \approx 0.6 - 1\text{m}$; for smaller and larger values of L_s there is a good agreement between the two resolutions. (b) Time-variation of the total amount of aerosol present within the computational domain for the two grid resolutions; the two curves are nearly identical for all times (t).

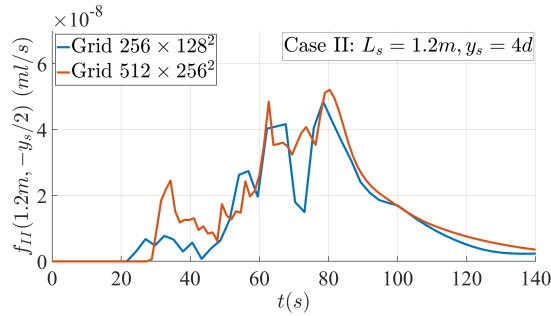


Figure S11: **(Grid resolution exercise)** Time-variation of aerosol flux, f_{II} (calculated from equation (1) in the main text), for Case II (conversation between two people) with $L_s = 1.2\text{m}$ and $y_s = 4d$ for two grid resolutions. The overall trends are similar but there are some quantitative differences for times close to 30s and 70s. Note that these variations are likely to be a result of the statistical variations between two simulations due to a sensitive dependence of turbulence on initial/boundary conditions, which can in principal be removed by ensemble averaging; also see the comments in Abkarian et al. (2020). As seen in Fig. S9, the energy dissipation is accurately captured, and therefore turbulence is well-resolved for both the grid sizes.

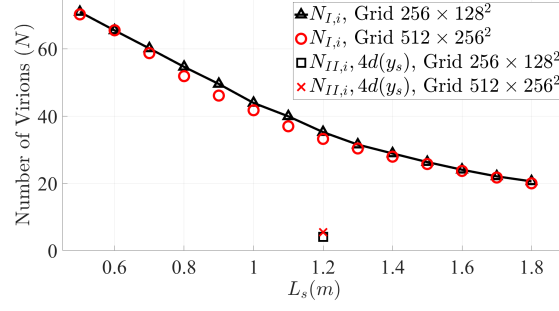


Figure S12: (Grid resolution exercise) The number of virions ingested by a listener located at a distance L_s from the speaker for Cases I and II, calculated (using equations (6) and (7) in the main text) for two grid resolutions. For Case II, we choose $y_s = 4d$, as for this parameter setting, although the two speech jets show some interference between them, a small number of aerosols manage to reach the other person's face (Fig. 4(d) in the main text). As can be seen, there is a good overall match between the number of virions between the two grid resolutions. For Case I, the maximum deviation is about 8%, whereas for Case II, there is a difference of one virion between the two resolutions. (Note that, for Case II, the number of virions reaching Person 2 is already sufficiently small, so a change of one virion does not have any effect on the risk of infection.)

3 Effect of buoyancy on the vertical deflection of speech flow

Figs. S13 and S14 show that the buoyancy due to temperature differences between the speech flow and the ambient air does not cause any perceptible vertical deflection of the flow.

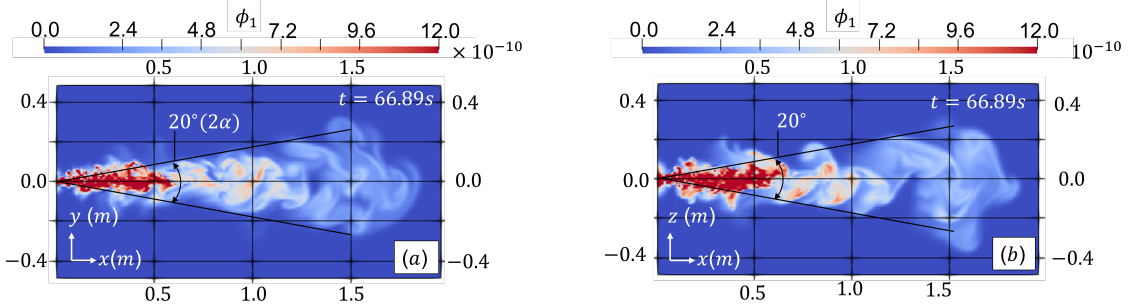


Figure S13: (Angle of spread of the speech jet) Distribution of aerosol concentration from Person 1 in (a) xy plane, and (b) xz plane (Case I). Abkarian et al. (2020) report the jet-angle to be about 20° (the range reported in Yang et al. 2020, is $20^\circ - 28^\circ$) defined as the conical region which contains 90% of the total scalar concentration. This cone angle, $2\alpha (= 20^\circ)$, is shown in the figure which is found to represent the spread of the speech jet quite well for $x \gtrsim 0.5m$ (i.e. after the self-similar regime begins; Fig. S15(b)). Furthermore, the jet is seen to spread nearly at the same angle in both xy (vertical) and xz (horizontal) planes. Also there is no visible deflection of the jet in the vertical direction, which suggests that buoyancy does not play an important role in the evolution of this flow. Thus the results obtained for a vertical separation between two people can be applied equally well to a lateral separation (i.e. in z direction) between them.

4 Comparison between top-hat and Gaussian profiles for a speech jet

In the following, we derive the relationships between the top-hat quantities used in Yang et al. (2020) and the Gaussian steady-jet quantities used in the present work, such as the centreline parameters and the “ $1/e$ width”. As defined in the main text, the $1/e$ width is a radial distance from the jet axis where a quantity drops to $1/e$ times of its centreline value. The Gaussian steady-state profiles of the time-averaged axial velocity and aerosol concentration are defined as:

$$\bar{u}_x(x, r) = U_c \exp(-(r/b_{ue})^2), \quad (S8)$$

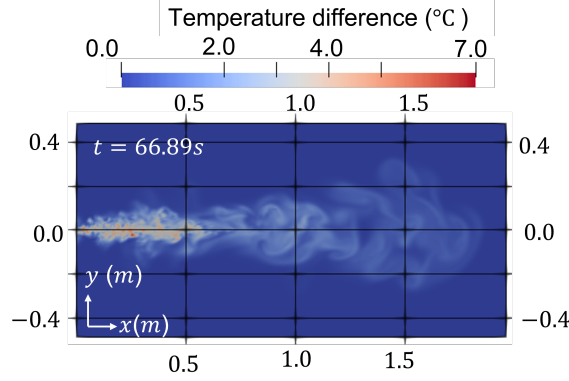


Figure S14: **(Temperature distribution for the speech flow)** Contour plot of temperature difference (ΔT) for the speech flow for Case I at $t = 66.89s$. Note that at the orifice, $\Delta T_o = 14^\circ C$. ΔT is seen to drop drastically over a short distance from the orifice so that for $x < 0.5m$ the maximum ΔT is less than half of ΔT_o . This is primarily due to the turbulent entrainment of ambient fluid into the speech flow causing it to spread laterally as it is issued from the orifice (Turner 1986). For $x > 0.5m$, the maximum ΔT is seen to be $< 4^\circ C$ indicating that the buoyancy forces are going to be small in this region further supporting the observation of Fig. S13.

$$\bar{\phi}(x, r) = \phi_c \exp(-(r/b_{\phi_e})^2). \quad (S9)$$

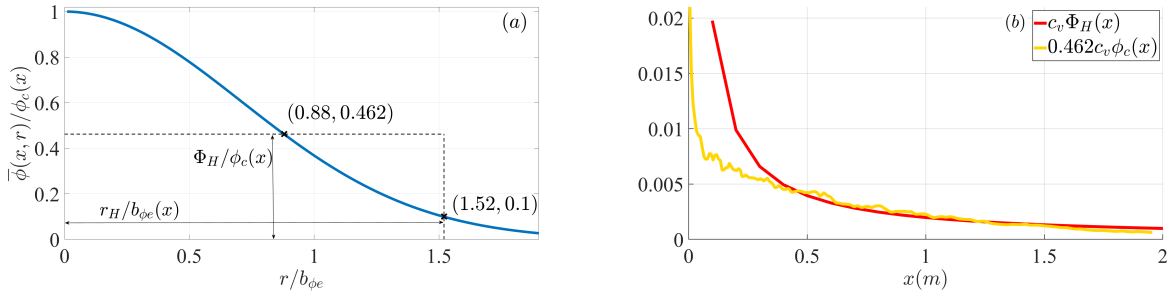


Figure S15: **(Graphical comparison of Gaussian and top-hat quantities)** (a) Gaussian distribution for the time-mean aerosol concentration $\bar{\phi}$, relating the characteristic Gaussian jet radius and centreline aerosol concentration (b_{ϕ_e} and ϕ_c) to the top-hat values of Yang et al. (2020). Φ_H is shown by the dashed top-hat profile over a radius of r_H/b_{ϕ_e} with a height equal to $0.462\phi_c$ (equation S17). This illustrates the likely underestimation of number of virions inhaled from the region near the jet axis for $r/b_{\phi_e} < 0.88$. (b) Comparison of the axial variation of the number density of virions ($c_v\phi$) between the top-hat and Gaussian distributions. With a pre-factor of 0.462 the Gaussian centreline number density matches well with the top-hat number density for $x > 0.45m$, which can be taken as the beginning of the steady self-similar regime for the simulated speech jet.

Here, b_{ue} and b_{ϕ_e} are the $1/e$ widths of axial velocity and aerosol concentration profiles respectively, and the overbar indicates time averaging. Yang et al. (2020) define the jet radius $r_H = x \tan \alpha$, based on the cone of half angle α which covers 90% of total passive scalar in it. The amount of scalar (or aerosols in the present context) in a circular area within a distance r from the axis is given by

$$G = \int_0^r \bar{\phi}(x, r) 2\pi r dr = \phi_c \pi b_{\phi_e}^2 [1 - \exp(-(r/b_{\phi_e})^2)]. \quad (S10)$$

Total amount of scalar could be found from integration over the whole planar area, i.e., r going from 0 to ∞ , as

$$G_{total} = \phi_c \pi b_{\phi_e}^2. \quad (S11)$$

To find r_H , we substitute $G = 0.9G_{total}$ in equation (S11). This along with equation (S10) leads to

$$0.9\phi_c\pi b_{\phi_e}^2 = \phi_c\pi b_{\phi_e}^2 [1 - \exp(-(r_H/b_{\phi_e})^2)]. \quad (\text{S12})$$

Equation (S12) gives us the relation between r_H and b_{ϕ_e} as $r_H = 1.516b_{\phi_e} = 1.819b_{ue}$. Here we have used $b_{\phi_e} = 1.21b_{ue}$, which is the standard relationship between the velocity width and passive-scalar width for a steady self-similar jet (Singhal et al. 2021). Next, we equate the integral momentum flux for the “top-hat” and Gaussian profiles, which is really one of the defining relations for the top-hat quantities (Turner 1986). This gives

$$U_H^2(x)A_H(x) = \int_0^\infty \bar{u}_x^2(x, r)2\pi r dr, \quad (\text{S13})$$

$$U_H^2(x)\pi[1.819]^2b_{ue}^2 = 0.5 * U_c^2\pi b_{ue}^2. \quad (\text{S14})$$

Here U_H and A_H are the top-hat jet velocity and area respectively. Equation (S14) gives the relation $U_H(x) = 0.39U_c$ between the top-hat and Gaussian velocity parameters. Next, we use the defining relation for the top-hat aerosol concentration to relate it to the centreline Gaussian aerosol concentration:

$$\Phi_H(x)U_H(x)A_H(x) = \int_0^\infty \bar{\phi}(x, r)\bar{u}_x(x, r)2\pi r dr, \quad (\text{S15})$$

$$\Phi_H(x)U_H(x)\pi[1.819]^2b_{ue}^2 = \phi_c U_c \pi \frac{b_{ue}^2 b_{\phi_e}^2}{b_{ue}^2 + b_{\phi_e}^2}, \quad (\text{S16})$$

$$\Phi_H(x) = 0.462\phi_c. \quad (\text{S17})$$

Thus, the top-hat aerosol concentration Φ_H used by Yang et al. (2020) has a much lower value than the centreline value for the Gaussian profile (ϕ_c). Fig. S15(a) shows a graphical relation between the top-hat and Gaussian profiles and Fig. S15(b) compares the number density of virions based on $\Phi_H(x)$ with that based on $\Phi_c(x)$.

5 Derivation of formula for Φ_{new}

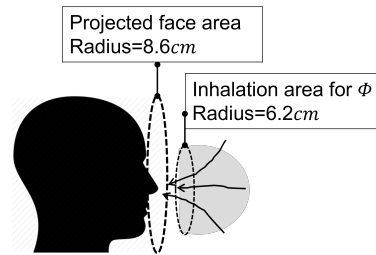


Figure S16: (Schematic representation of regions of interest for infection risk estimation) The circular region with a radius of 8.6cm shows the total projected area of the human face and is employed in calculation of infection through eyes and mouth. The hemisphere shown in grey depicts the region influenced by inhalation in a single breath. We use a circular region with the same radius as the hemisphere (= 6.2cm) to find the average scalar value Φ_{new} available for inhalation. The radii of circular regions and distances between them are not to the scale.

As mentioned in the main text, during inhalation, a person draws air from a circular region of radius 6.2cm having its center coinciding with the jet axis (Fig. S16). The average value of the aerosol concentration over this circular region (Φ_{new}) is obtained as:

$$\int_0^{6.2\text{cm}} \bar{\phi}(x, r)2\pi r dr = \Phi_{new}\pi(6.2)^2. \quad (\text{S18})$$

Substituting $\bar{\phi}(x, r)$ from equation (S9) we get

$$\Phi_{new}\pi(6.2)^2 = \phi_c(x)\pi b_{\phi_e}^2 [1 - \exp(-(6.2/b_{\phi_e})^2)] . \quad (\text{S19})$$

This gives

$$\Phi_{new} = (b_{\phi_e}/6.2)^2 [1 - \exp(-(6.2/b_{\phi_e})^2)] \phi_c. \quad (\text{S20})$$

To convert b_{ϕ_e} in terms of axial distance, the relation $b_{\phi_e} = 0.137(x - x_o)$ mentioned in Singhal et al. (2021) is used.

Supplementary movies

Movie S1. Time evolution of speech jets from two people in conversation (Case II) for different y_s and $L_s = 1.2\text{m}$.

Movie S2. Time evolution of speech jets for Case II (involving speech asymmetry) compared with Case II (involving symmetric speech durations) for $L_s = 1.2\text{m}$ and $y_s = 0$.

Movie S3. Time evolution of speech jets from two people in conversation (Case II) for $L_s = 0.6\text{m}$ and $y_s = 0$, highlighting the highly oscillatory interaction between the jets.